



# Impact of pump phase modulation on QAM signals in polarization-insensitive fiber optical parametric amplifiers

M. Bastamova<sup>\*</sup>, V. Gordienko, N.J. Doran, A.D. Ellis

Aston Institute of Photonic Technologies, Aston University, Birmingham B4 7ET, UK

## ARTICLE INFO

### Keywords:

Optical fiber parametric amplifiers  
Pump phase modulation  
Pump dithering  
QAM signals  
polarization-insensitive FOPA

## ABSTRACT

We examine mitigation of stimulated Brillouin scattering (SBS) in fiber optical parametric amplifiers (FOPAs) by pump phase modulation in the context of QAM signals and the state-of-art polarization-insensitive FOPA architecture. We characterize the impact of the pump phase modulation on QAM signals in the cases of single-polarization FOPAs and polarization-insensitive FOPAs, and study pathways to minimization of this impact. We find that the impact of pump phase modulation on signals is more complicated in polarization-insensitive FOPAs than in single-polarization FOPAs, and it can be mitigated by using the features of the polarization-insensitive FOPA architecture. We use the required optical signal to noise ratio (rOSNR) to evaluate the impact of pump phase modulation on QAM signals and find that the induced signal phase modulation makes significantly more contribution than the induced signal amplitude modulation. Our numerical and experimental study has revealed a distribution of the rOSNR penalty across the FOPA gain spectrum which is distinct from previously reported for on/off signals. We explore and optimize the pump phase modulation schemes to reduce the signal rOSNR penalty whilst providing more SBS mitigation at the same time. We demonstrate that a receiver digital signal processing plays a significant role in contribution to rOSNR penalty.

## 1. Introduction

The demand for high-speed data transmission is at an all-time high due to the ongoing digital revolution. The communication industry faces significant challenges due to the exponential growth in data traffic and the ensuing need for higher capacity and transmission rates [1]. These challenges can be effectively addressed by expanding the bandwidth employed by fiber optical communications into new bands. Fiber optical amplification is the enabling technology for this expansion in both long-haul systems and networks, therefore one of the major research topics today is the development of novel optical amplifiers enabling broadband low-noise amplification beyond the EDFA-enabled C&L bands [2–4]. Fiber optic parametric amplifiers (FOPA) attract a particular interest in this context for their unmatched abilities for amplification across multiple bands [5] and with ultra-wide bandwidth [6].

FOPA has a range of unique features enabled by their underlying principle of operation – four wave mixing (FWM). FOPA can provide theoretically unlimited bandwidth of operation [7,8] experimental demonstrations have shown its functionality in the S, C, and L bands [9,10,11]. FOPA is capable of phase-sensitive amplification [12]. Thus,

phase-sensitive FOPA has demonstrated a noise figure below 3 dB [13] unreachable by any other amplification technologies. Besides, a huge gain up to 70 dB has been experimentally demonstrated in [14] which is very difficult to achieve in most other amplification technologies. FOPA has recently matched the EDFA performance and is on the route to outperform it in ultra-fast transient-free applications [15,16].

Recent advancements in FOPAs have addressed issues of polarization-insensitive, low noise and crosstalk operation. Indeed, the polarization-insensitive FOPA (PI-FOPA) ability for broadband and high output power operation has been demonstrated in [17]. However, FOPA performance is limited by drawbacks of stimulated Brillouin scattering (SBS) mitigation which is strictly necessary for FOPA operation [18,19]. Several techniques have been employed in the past twenty years to mitigate the SBS: changing the core diameter along the length of a fiber [20], changing the dopant concentration in the fiber [21], introducing temperature gradients along the fiber [22,23], designing acoustically guiding and antiguiding refractive index profile [24], introducing longitudinal strains [25], using isolators [26], and Fiber Bragg Gratings [27]. However, these techniques have not allowed achievement of broadband FOPA gain spectrum due to insufficient SBS mitigation,

<sup>\*</sup> Corresponding author.

E-mail address: [210114416@aston.ac.uk](mailto:210114416@aston.ac.uk) (M. Bastamova).

<https://doi.org/10.1016/j.yofte.2024.103758>

Received 6 December 2023; Received in revised form 18 February 2024; Accepted 22 March 2024

Available online 3 April 2024

1068-5200/© 2024 The Authors. Published by Elsevier Inc. This is an open access article under the CC BY license (<http://creativecommons.org/licenses/by/4.0/>).

induced longitudinal dispersion variation and complexity. Therefore, the most practical approach to significantly increase the SBS threshold up to 20 dB and to allow for a large FOPA net gain remains to be pump phase modulation, known as dithering [28,29]. Pump phase modulation allows to increase pump bandwidth beyond Brillouin interaction bandwidth for reduction of the Brillouin gain obtained by the incident laser. By applying this method, the SBS is effectively suppressed without causing the pump amplitude modulation (except for a small residual pump amplitude modulation [30]).

It has been shown that the pump dithering induces an instantaneous pump frequency modulation and causes gain fluctuations in FOPA degrading amplified signals [31]. The degradation reached up to 10 dB penalty of the signal quality factor ( $Q^2$ ) produced by gain fluctuations caused by pump frequency or power variations, in single and double-pumped FOPA devices [32]. There are several ways of implementing pump phase modulation in FOPA, whereas pump is phase modulated with pseudo random bit sequence (PRBS) [31], sine tones [28], thermal noise [33]. Phase modulation of the pump by PRBS introduces significant distortions in gain leading to decrease in signal SNR [31,34–36] compared to modulation with several sine tones for both OOK [34] and PSK [35] signal modulation formats. While in two-pump FOPA counter-phase modulation allows to reduce the impact of pump phase modulation significantly [34], the requirement to produce pumps in unfavorable wavelength ranges limits two-pump FOPA ability to operate across wide bandwidth. Moreover, two-pump FOPAs induce more nonlinear crosstalk than single-pump FOPAs [6].

However, most studies referred to basic modulation formats (OOK, PSK) in single-polarization FOPAs, so the impact of dithering on coherent detected modulation formats in PI-FOPAs remained unexplored. Our preliminary study has shown that coherently-detected QAM signals experience a very different behavior than directly-detected ASK and BPSK signals for two reasons: on the one hand, coherent detection reduces the impact of the power gain fluctuations because coherent detectors refer to optical field amplitude rather than optical power; on the other hand, QAM signals are susceptible to phase noise introduced by FOPAs with pump phase modulation [37]. Therefore, the impact of pump phase modulation in FOPA on QAM signals must be examined separately. Moreover, the impact of pump phase modulation has not been studied in PI-FOPAs at all.

In this work we extend our previous theoretical study of the required optical signal to noise ratio (rOSNR) penalties for PDM-16QAM signals induced by the pump phase modulation in FOPAs [37] with experiments and simulations taking into account performance of commercial coherent receivers and features of a FOPA polarization-insensitive architecture [17]. For the first time, to the best of our knowledge, we experimentally confirm that QAM signal quality penalties due to pump dithering are dominated by the induced signal phase modulation rather than by the induced amplitude modulation. Therefore, QAM signal penalties have different distribution across the FOPA gain spectrum than previously studied in detail OOK signals. The impact of pump phase modulation has been examined by employing different multi-sinusoidal waveforms to estimate the SBS suppression effectiveness and we find that larger number of tones with less frequency spacing between them facilitates better signal OSNR for the same or better SBS mitigation.

We investigated the impact of pump phase modulation on polarization-multiplexed signals in a PI-FOPA for the first time. We find that PI-FOPAs even employing a single pump allow for compensation of the impact of dithering if pumps in different arms of a polarization insensitive architecture appear in counter-phase.

## 2. Theory of pump phase modulation in single-polarization FOPA

### 2.1. Pump phase modulation

The pump dithering effectively mitigates SBS by broadening the

pump beyond the Brillouin gain bandwidth. As the power of a pump phase modulated with sine tones remains constant, its power is uniformly distributed between equally spaced discrete lines in the frequency domain. Pump phase modulation with sinusoidal tones can be very effective because it provides control over the pump bandwidth and uniformity of the spectrum by applying a voltage of 1.4 V<sub>pi</sub> for each individual tone [28]. Moreover, a FOPA employing a pump phase modulated with tones demonstrated to preserve signal quality better than with PRBS [31,35]. Given that modulation with tones is deterministic, one can identify additional possibilities, such as the potential for complete cancellation of the dithering effect. For example: counter-phase modulation in two-pump FOPA [34].

Pump phase modulation with an amplitude of  $\sim 1.4$  rad per tone splits the pump into 3 equal power lines of zero and first orders spaced with the modulation frequency. Each additional tone splits every line produced by previous tones in three equal lines as well, i.e. producing beat frequencies. Therefore, pump phase modulation with  $N$  sine tones in the electrical frequency spectrum splits the pump into  $3^N$  first order lines in optical spectrum. The high order harmonics are much weaker, so we do not take them into account. If the frequency of the  $n$ -th tone is three times the frequency of the  $(n-1)$ -th tone, then all first order lines are equally spaced with the frequency of the lowest tone, which we call the base tone [28]. However, sine tones with a non-integer multiplication factor (e.g. 3.05) between them prevent first order lines from overlapping with higher order lines, resulting in flatter pump spectrum and, hence, a more efficient SBS mitigation. If the base tone frequency is larger than the Brillouin gain bandwidth, then the pump power is split between  $3^N$  tones which do not interact via Brillouin, and consequently the SBS threshold increases by a factor of  $3^N$ . A typical Brillouin gain bandwidth for a HNLF is between 20 MHz and 50 MHz [28,38]. In theory a SBS threshold increase by a factor of 10 typically gives a single stage amplifier gain up to 20 dB, while in practice the SBS threshold increase by a factor of  $\sim 20$  is required [19]. Three tones allow the SBS threshold to be increased by a factor up to 27. We have observed that the SBS threshold is an approximately 4 dB higher when using tones with a non-integer multiplication factor than with an integer multiplication factor due to the improved flatness enabled by avoiding interference with higher order harmonics. Indeed, the multiplication factor should be close to 3 to allow for almost equal spacing between the first-order harmonics and their combinations and thus to achieve the highest bandwidth efficiency.

Pump phase  $\varphi_p$  modulated with  $N$  sinusoidal tones is shown by equation (1), where  $Am$  is the phase modulation amplitude, and the  $fm_n$  is the modulation frequency of the  $n$ -th tone. Modulation amplitude  $Am$  is generally the same for all tones and set at  $\sim 1.4$  rad which is the cross point of the Bessel functions  $J_0$  and  $J_1$  leading to equal power of the carrier and the side lobes. We define the total pump bandwidth as the bandwidth occupied by the first order lines. It is equal to twice the sum of all modulation frequencies  $fm_n$ .

$$\varphi_p(t) = Am \bullet \sum_{n=1}^N \sin(2\pi \bullet fm_n \bullet t) \quad (1)$$

Importantly, the pump phase modulation can be viewed as an instantaneous pump frequency modulation shown by Eq. (2), where  $f_p$  is the central pump frequency and  $Am \bullet \sum_{n=1}^N fm_n \bullet \sin(2\pi \bullet fm_n \bullet t)$  is the first derivative of the pump phase  $d\varphi_p(t)/dt$  divided over  $2\pi$  to convert from angular to ordinary frequency.

$$f(t) = f_p + Am \bullet \sum_{n=1}^N fm_n \bullet \sin(2\pi \bullet fm_n \bullet t) \quad (2)$$

### 2.2. Impact of pump phase modulation on QAM signals

We assess the influence of pump phase modulation in FOPA on coherently-detected QAM signals by analyzing the complex amplitude

gain rather than power gain, because coherent detection of QAM signals refers to a signal complex amplitude rather than the signal power [39]. In other words, the complex amplitude gain combines the FOPA impact on both signal amplitude and phase: its modulus defines a signal amplification, and its argument defines an induced phase shift. The complex amplitude gain  $h_3$  in FOPA is defined as the ratio between complex amplitudes of output and input signals,  $A_{out}$  and  $A_{in}$  respectively (the nomenclature is taken from [7]). The solution for the no fiber loss, no pump depletion case is shown by Eq.(3) [7], where  $L$  is the gain fiber length,  $P$  is the pump power,  $\gamma$  is the gain fiber nonlinearity coefficient,  $g = \sqrt{(\gamma \cdot P)^2 - k^2/4}$  is the gain coefficient and  $k = 2\gamma \cdot P + \beta_2 \cdot \Delta\omega^2$  is the total propagation constant.

$$h_3 = \frac{A_{out}}{A_{in}} = \left[ \cosh(g \cdot L) + i \frac{k}{2g} \sinh(g \cdot L) \right] \times \exp \left[ i \left( 2\gamma \cdot P - \frac{k}{2} \right) L \right] \quad (3)$$

The total propagation constant  $k$  is the key parameter defining the impact of the pump phase modulation on signal because it depends on the group velocity dispersion  $\beta_2$  at the pump frequency and the frequency detuning  $\Delta\omega$  between a signal and the pump. Both  $\beta_2$  and  $\Delta\omega$  vary in time due to instantaneous pump frequency modulation. Therefore, the total propagation constant  $k$  and consequently the gain coefficient  $g$  are time dependent.

We have performed simulations for three pump phase modulation scenarios to demonstrate and compare the instantaneous pump frequency modulation, the corresponding induced modulation of the complex gain  $h_3$  and the resulting impact on the 16QAM signal constellation diagram. We considered the pump phase modulation with one of three waveforms for each scenario. Each waveform was a combination of 4 sine tones, whereas the base tone was one of 25 MHz, 40 MHz or 85 MHz in the electrical frequency spectrum and higher frequencies were obtained via multiplication by 3.05, 3.05<sup>2</sup> and 3.05<sup>3</sup>. We set modulation amplitude of 1.4 rad per tone in all simulations. The corresponding total pump bandwidths calculated as twice 25 MHz times (1 + 3.05 + 3.05<sup>2</sup> + 3.05<sup>3</sup>) are 2086 MHz, 3338 MHz, 7094 MHz. We used 4 tones because it is the lowest number of tones allowing to achieve the required SBS threshold increase be a factor of  $\sim 20$  when using base tone frequency of 25 MHz.

Fig. 1(a) shows traces of the pump frequency detuning from the unmodulated pump frequency and the corresponding  $|h_3|$  and  $\arg(h_3)$  versus time. The pump frequency over time was calculated using Eq. (2). The complex gain  $h_3$  was calculated with Eq. (3) for the pump wavelength of 1566.2 nm, fiber zero-dispersion wavelength (ZDW) of 1562.9 nm, fiber dispersion slope of 43 s/m<sup>-3</sup>, pump power of 4.3 W, HNLf length of 50 m,  $\gamma$  of 14 W<sup>-1</sup>km<sup>-1</sup>. The  $|h_3|$  is the square root of the power

gain, so  $|h_3|$  of  $\sim 10$  dB corresponds to the power gain of  $\sim 20$  dB. The pump frequency modulation transfers to  $h_3$ : its modulus  $|h_3|$  varies in-phase with pump frequency with peak-to-peak amplitude of 0.11 dB for  $f_{\text{base tone}}$  of 25 MHz and of 0.57 dB for  $f_{\text{base tone}}$  of 85 MHz. Phase shift of  $h_3$  varies in counter-phase with peak-to-peak amplitudes of 0.075 rad and 0.37 rad responsibly.

Fig. 1(b) shows the impact of induced modulation of  $|h_3|$  and  $\arg(h_3)$  on a constellation of 16QAM signal amplified by FOPA. This was calculated as follows. The complex amplitude gain  $h_3$  was calculated for 1000 uniformly spaced time points across a time frame of 100 ns. This array of complex gains was multiplied with an array of 16 signal complex amplitudes corresponding to the 16QAM constellation points (input signals) to obtain an array of output signal complex amplitudes. Then, the array of output complex amplitudes was normalized by dividing it over average complex amplitude gain  $\langle |h_3| \rangle \cdot \exp(\langle \arg(h_3) \rangle)$ , which is equivalent to signal attenuation by the average gain value and subsequent phase recovery in a signal transmitter. The result is shown at Fig. 1(b). It demonstrates that the induced phase modulation is dominant over the induced amplitude modulation, and it scales dramatically with increase of pump bandwidth. Finally, a white Gaussian noise has been added to the array of signal complex amplitudes to set the SNR of 25 dB for this demonstration. Fig. 1(c) confirms that the induced phase noise is the major source of 16QAM signal degradation due to pump phase modulation in FOPA.

We further characterize the impact of pump phase modulation by introducing the required-OSNR penalty (rOSNR) defined as the OSNR difference between the simulated BER curve with FOPA and the theoretical (back-to-back) curve at the BER level of 0.01. The simulated BER with FOPA was calculated using an error probability function for each of 16x1000 complex signal amplitudes calculated above and a range of SNR values similarly to [37]. Grey coding has been assumed when calculating BER from symbol error rate.

Fig. 2(a) demonstrates spectra of the modulus and the argument of  $h_3$  calculated with parameters from Fig. 1, whereas Fig. 2(b) shows rOSNR penalty simulated for a range of signal wavelengths across the FOPA gain bandwidth and for waveforms employing 3 and 4 tones with frequency ratios of 1, 3.05, 3.05<sup>2</sup> and 3.05<sup>3</sup>. The rOSNR penalties appear to increase with the total pump bandwidth regardless of base tone frequencies and number of employed tones. Observed signal penalty distribution across the FOPA gain bandwidth differs from previously reported Q<sup>2</sup> penalties which were minimal at the gain peak and have two maxima at the FOPA gain slopes [32]. Our simulated penalties demonstrate minimum at the vicinity of pump wavelength (1566.2 nm) and increase significantly with signal detuning from the pump. The wavelength range of the largest rOSNR penalty is observed where  $|h_3|$  has the

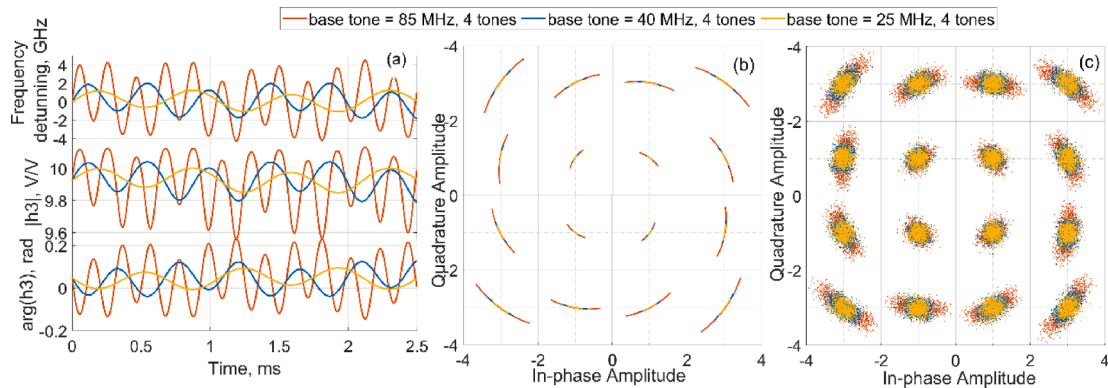
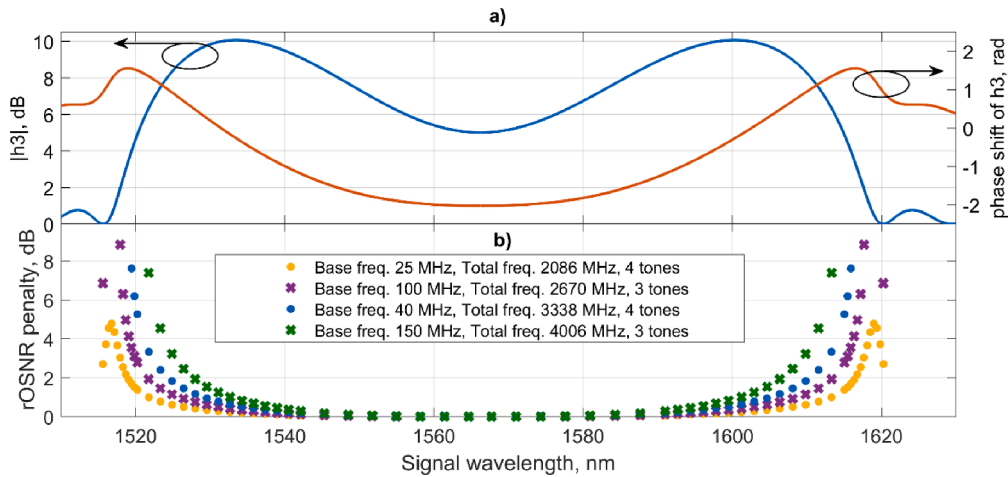


Fig. 1. A) timeline of the pump frequency detuning due to phase dithering,  $|h_3|$  and  $\arg(h_3)$ ; b) constellation diagram of amplified a 16QAM signal by FOPA. c) Same diagram with added white noise equivalent to an SNR of 25 dB. FOPA parameters for pump wavelength of 1566.2 nm, fiber zero-dispersion wavelength (ZDW) of 1562.9 nm, fiber dispersion slope of 43 s/m<sup>-3</sup>, pump power of 4.3 W, HNLf length of 50 m,  $\gamma$  of 14 W<sup>-1</sup>km<sup>-1</sup>. No loss, no pump depletion case. Pump phase modulation base tones of 25 MHz (yellow), 40 MHz (blue) and 85 MHz (red). Signal frequency 195.8 THz. (For interpretation of the references to colour in this figure legend, the reader is referred to the web version of this article.)



**Fig. 2.** A) modulus  $|h_3|$  (blue) and phase shift of  $h_3$  (red) calculated with parameters from Fig. 1 and b) rOSNR penalty vs wavelengths for 4 pump modulation waveforms employing 3 tones with  $f_{\text{basetone}}$  of 100 MHz and 150 MHz (crosses) and 4 tones with  $f_{\text{basetone}}$  of 25 MHz and 40 MHz (dots). (For interpretation of the references to colour in this figure legend, the reader is referred to the web version of this article.)

largest slope and  $\arg(h_3)$  reaches the maximum. The rOSNR curve does not have a minimum at gain peaks as in previous studies focused on basic modulation formats [32] because quadrature-modulated signals are susceptible to induced signal phase modulation. The correlation between curves for the rOSNR penalty and the phase shift implies that the induced phase noise is the major source of 16QAM signal degradation due to pump phase modulation in FOPA.

Note, here and further we only consider an impact of pump phase modulation on signals and neglect an impact of residual pump amplitude modulation, because we have experimentally measured that the residual pump amplitude modulation of a pump phase-modulated with our commercially sourced phase modulator is  $-60$  dB per tone, and our simulations showed that it has a negligible impact on the FOPA gain and the rOSNR of the amplified signal.

### 2.3. Impact of pump dithering in looped PI-FOPA

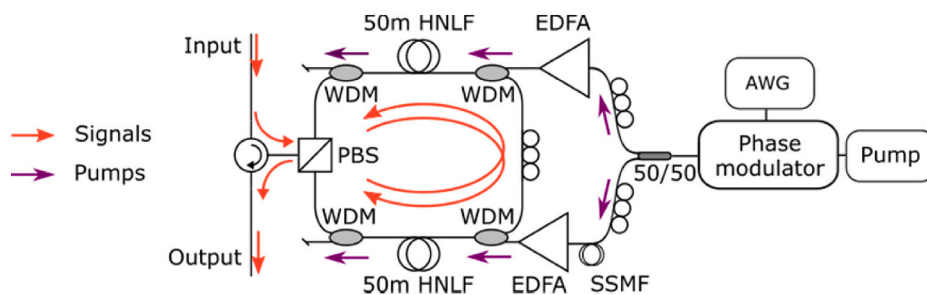
In this section we extend our model of required-OSNR penalties for 16QAM signals induced by the pump dithering in FOPAs considering features of polarization-insensitive Looped FOPA architecture (PI-FOPA) [17]. A signal in single-pump Looped PI-FOPA is split by a polarization beam splitter (PBS) into orthogonal linearly polarized components counter-propagating in a loop, and both components are independently but equally amplified within the loop before being recombined by the same PBS. The loop employs two nominally identical gain fibre lengths each pumped unidirectionally from one phase modulated pump laser [17].

Fig. 3 shows that once the pump is split by a 3 dB coupler, the two patchcord lengths of fibers that deliver pump power to HNLF are not deliberately length-matched. That means the pump phase modulation waveforms and consequently distortions induced on the signal

components might be not synchronized in the gain fibres, and moreover the delay between them is prone to drifting over time. Therefore, the signal components are split between two spatial parts and receive a different phase and amplitude shift depending on the instantaneous pump frequency shift in each arm at every moment. Hence, upon recombination of the amplified signal components, the signal distortion caused by pump phase modulation in looped PI-FOPAs is a linear combination of the signal distortions in each arm of the PI-FOPA yet with a delay between them. This is more complicated than in previously studied single-polarization FOPAs and opens ways for compensation of the signal distortion caused by the pump phase modulation in PI-FOPAs.

The impact of asynchronization between the pumps on the overall system performance depends on how a signal is split by the PBS. Assume a polarization division multiplexed signal, its components can be split equally, asymmetrically or aligned to PBS axes. If a PDM signal consists of a single component, that component can also be either divided or directed into one of two distinct spatial paths. However, in practice, PDM signal components split with a random factor between two paths in PBS.

If the pumps' modulation is in phase (i.e. pump optical paths are matched) both signal components experience the same distortion, and this is largely the same as in single-polarization FOPAs. If the polarization multiplexed signal components are aligned to the PBS axes, then pump synchronization has no impact on constellations of the signal components as each is amplified by a separate pump. However, in most cases two parts of the signal will inherit different modulations in each spatial paths and the result will be averaged upon recombination in the PBS. If pumps' modulation is in counter phase and the signal components are split equally between the spatial paths, the inherited modulation in theory can be completely cancelled out. Therefore, there are two steps towards cancelling the inherited modulation: to control



**Fig. 3.** Scheme of PI-FOPA with different fiber lengths between fiber coupler and EDFAs. PBS – polarization beam splitter, AWG – arbitrary waveform generator.

splitting of PDM signals in PBS and to adjust phase relation between pump optical paths.

#### 2.4. Mitigation of the dithering impact in looped PI-FOPA

The impact of dithering can be cancelled in a single-pump looped PI-FOPA by ensuring that the impact of dithering on signal phase and amplitude is opposite in the PI-FOPA arms and the polarization components of the signal are split equally between arms. The opposite impact of dithering can be achieved thanks to the periodic nature of tones used for pump phase modulation by introducing a half period delay between pumps in the gain fibres. Half period delay is 4 m of fiber length for multiple tones with  $f_{\text{basetone}}$  of 25 MHz. However, one requires hundreds of kilometers to create half period delay between pumps for unmultiple tones which is practically inconvenient. Nevertheless, it is still possible to significantly mitigate impact of dithering as the required delay to get minimum penalty can be adjusted to the provided optical path mismatch by adjusting tones' frequencies.

Given that the required delay between the pumps is achieved in the gain fibres, mitigation of the impact of dithering requires to split signal polarization equally between the PI-FOPA arms. This issue can be solved by adding a polarization tracker to set and maintain the target polarization at the FOPA input [40]. Alternatively, signal polarization can be randomized with a polarization scrambler to provide some mitigation of the dithering impact as compared to the 'single-polarization' case.

Fig. 4 shows a PI-FOPA  $|h_3|$  and  $\arg(h_3)$  calculated over time for the above-mentioned scenarios as a weighted sum of complex gains in each arm, where weighting factors  $K$  and  $1 - K$  represent the fraction of signal power in each PI-FOPA arm. The pump was phase modulated with 4 tones with base frequency of 25 MHz and frequency ratios of 1, 3.05, 3.05<sup>2</sup> and 3.05<sup>3</sup>. We consider two cases: when the pumps in the gain fibers are either in phase or in counter-phase. For each case we assume the signal polarization is either aligned to one of PBS axes ( $K = 1$ ) or aligned with an angle of 45 degrees to the PBS axes and therefore signal power split equally between FOPA arms ( $K = 0.5$ ) or varies randomly

over time ( $K - \text{random}$ ). In the latter case  $K$  was described as beta distribution defined on the interval  $(0, 1)$  with parameters  $\alpha = 3/2$  and  $\beta = 3/2$  imitating distribution of polarization states over Poincare sphere and calculated for  $N = 1000$  points. We consider that polarization changes slow as compared to the symbol rate, but fast enough to observe averaging of BER within an error counting window.

When the pumps are in-phase, the fluctuations of the PI-FOPA gain modulus and phase shift are independent of how signal components are split by the PBS and they are the same in a single-polarization FOPA. However, when the pumps are in counter-phase, fluctuations of the PI-FOPA gain are reduced in some cases. The alignment of signal component's polarization with PBS axes ( $K = 1$ ) causes the same fluctuation of FOPA gain even if pumps are in counter-phase. When signal component's polarization is equally split between PBS axes ( $K = 0.5$ ), fluctuation of FOPA gain is noticeably suppressed: peak-to-peak amplitude of  $|h_3|$  decreased from 0.16 dB to 0.04 dB and peak-to-peak amplitude of  $\arg(h_3)$  decreased from 0.1 rad to 0.025 rad. If the polarizations of PDM signals are not controlled, they can undergo random fluctuations over time, enabling averaging between the two previous scenarios and partially mitigating the impact of dithering.

Fig. 5 shows that in case of the random signal polarization ( $K$  random, yellow) the distributions of both gain modulus  $|h_3|$  and phase shift  $\arg(h_3)$  are significantly narrower than in case of the signal copolarized with one of PBS axes ( $K = 1$ , blue). Therefore, the general case of randomly varying input signal polarization in a PI-FOPA provides less scattering of an amplified signal complex amplitude than the worst-case scenario equivalent to a single-polarization FOPA.

Fig. 6 shows rOSNR penalty as a function of signal wavelength for three scenarios:  $K = 1$  (blue),  $K = 0.5$  (red) and  $K - \text{random}$  (yellow), calculated for FOPA and phase modulation parameters from Fig. 1. The rOSNR penalty calculated for  $K = 1$  demonstrates the highest level of penalty the same as single-polarization FOPA on Fig. 2. All other scenarios are better. Splitting PDM signals equally in PBS allows to decrease penalty below 0.005 dB across all examined wavelengths. Randomly scrambling polarization of PDM signal components minimizes rOSNR

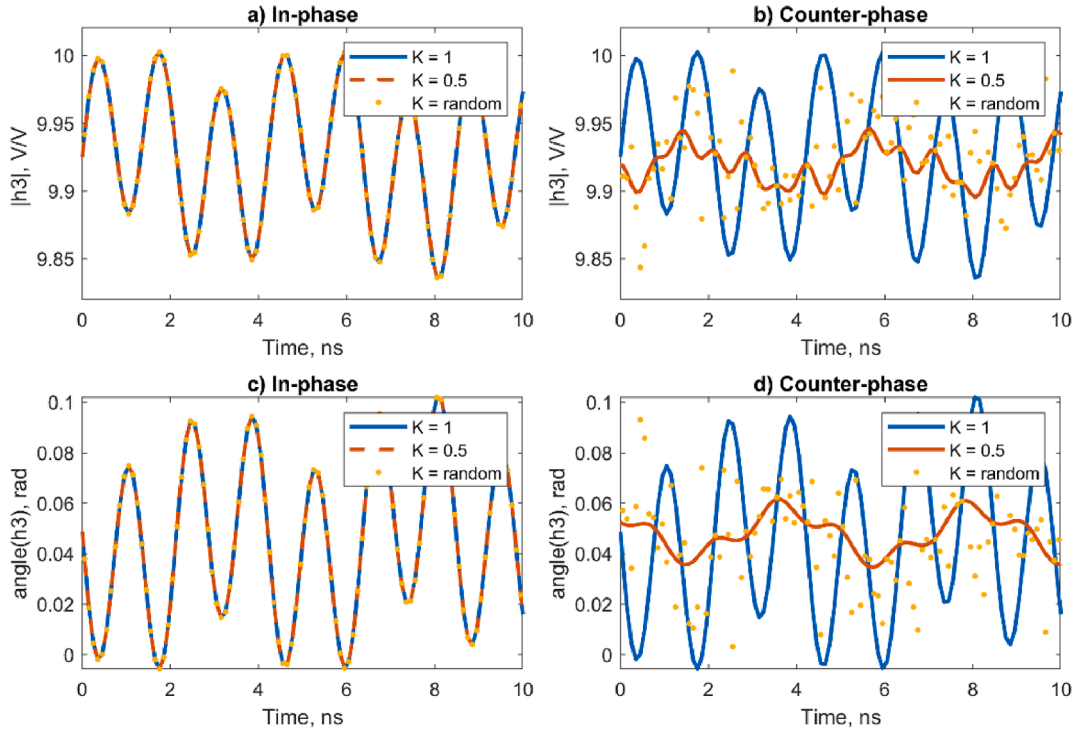


Fig. 4. PI-FOPA gain modulus  $|h_3|$  when pump modulation waveforms are a) in-phase, b) counter-phase and Phase shift  $\arg(h_3)$ : c) in-phase, d) counter-phase for three different  $K$  factors of 1, 0.5 and randomly distributed in range  $[0,1]$ .  $|h_3|$  and  $\arg(h_3)$  are calculated using the parameters from Fig. 1 with pump phase modulation employing 4 tones, with a  $f_{\text{base tone}} = 25$  MHz.

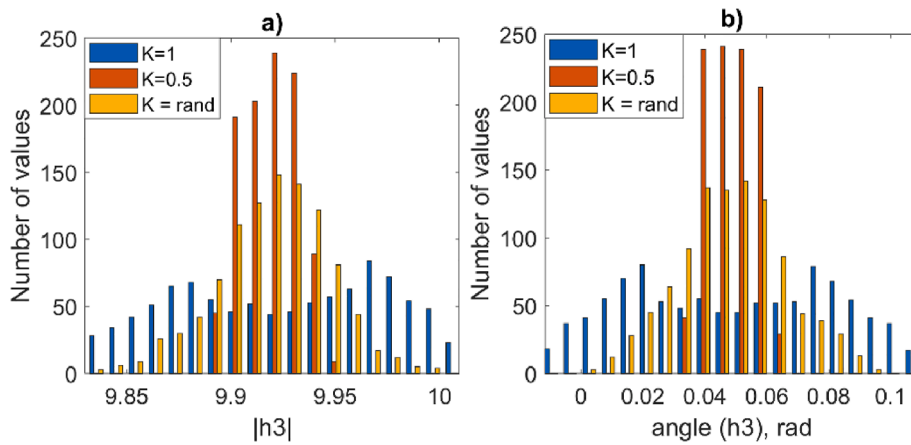


Fig. 5. Distribution of  $|h_3|$  and  $\arg(h_3)$  when pump modulation waveforms are counter-phase for different K factors. Distribution of pump modulation waveforms are in-phase coincide with the case of  $K = 1$ .

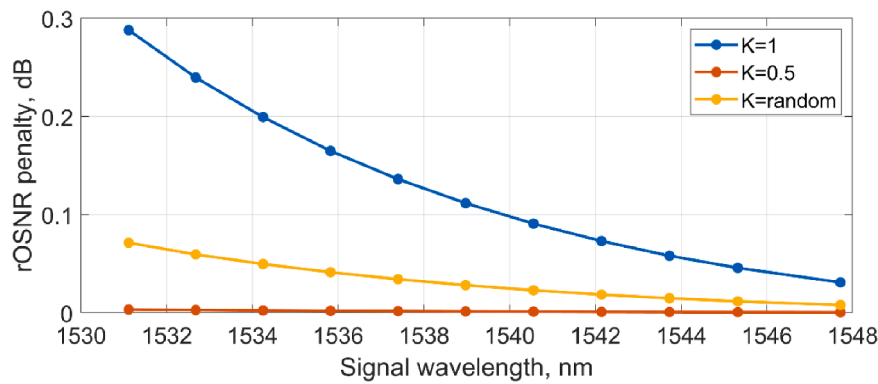


Fig. 6. rOSNR penalty versus Signal wavelengths for three K factors of 1, 0.5, random. Pump optical paths are in counter-phase. Plots are simulated using the parameters from Fig. 1 with pump phase modulation employing 4 tones, with  $f_{\text{basetone}} = 25$  MHz.

penalty below 0.1 dB. It can be explained as polarization fluctuations are more likely to approach  $K = 0.5$  than  $K = 0$  or 1 since there are only two points on the Poincaré sphere where polarization aligns with the PBS axes.

Therefore, if we do a small effort to have the required optical pump path difference, we already improve on the FOPA performance. Thus,

Fig. 7 shows the rOSNR penalty as a function of the optical pump path difference and the base tone frequency assuming  $K = 0.5$  and demonstrates that either the optical path difference or the base tone frequency can be adjusted slightly to get rOSNR penalty below 0.05 dB. Generous margin of optical path difference  $\sim 14$  cm and base tone frequency margin of 0.8 MHz allows for maintaining penalty level below 0.1 dB.

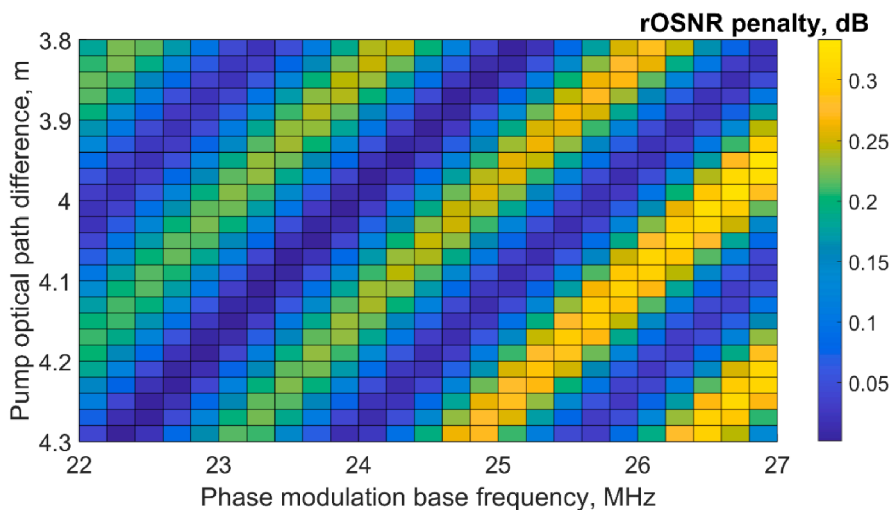


Fig. 7. rOSNR penalty calculated for a range of the pump phase modulation base tone frequencies and the pumps' optical path differences. Diagram is simulated using the parameters from Fig. 1 with pump phase modulation employing 4 tones with  $f_{\text{basetone}} = 25$  MHz.

### 3. Experimental study of pump dithering in looped PI-FOPA

#### 3.1. Evaluating $rOSNR$ penalty with Real-World receivers

In this subsection we examine the impact of an induced signal phase and amplitude modulation on a commercial receiver BER. Inclusion of this data into our simulation model instead of an ideal receiver will improve our simulation model and allow for comparison between our simulated and experimental results. We investigate the impact of the signal phase and amplitude modulation on performance of a commercial receiver by measuring the required received (rRx) power penalty in B2B configuration when a small phase or amplitude modulation with a sine wave is applied to the signal. We define the rRx penalty as the difference between the required receiver power to achieve BER of 0.01 with and without the sine wave modulation. We consider the measured in this subsection rRx penalty to be equivalent to the rOSNR penalty under condition that the received signal SNR is limited by the receiver noise in the former case and by the optical noise in the latter case.

We have performed back-to-back measurements with a commercial line card for signal with and without external phase or amplitude modulation. We have introduced an external phase or amplitude modulation by inserting a phase or amplitude modulator prior to the transmitter IQ modulator (see Fig. 8). A polarization controller was added after the external modulator to set correct polarization for the IQ modulator. The external phase or amplitude modulator was driven with a single sine tone from an arbitrary waveform generator (AWG). Its power was adjusted with RF amplifier and RF attenuator to control power at the receiver. We have varied the amplitude of the induced signal phase and amplitude modulation and measured the required Rx power to achieve BER of 0.01 for the 35 GBaud PDM-16-QAM signal. The tone modulation frequency has been varied up to 4 GHz as well, but we found that it did not have an impact on the results.

Fig. 9 shows the linecard rRx penalty depending on the induced (a) phase modulation and (b) amplitude modulation penalty with linear approximation. We observed the rRx power to increase by 0.2 dB even without any modulation employed. This is the implementation penalty, which we subtract from the results. We have done 5 measurements for each point, whereas the black dot shows the average value, and the error bars show the standard deviation. Best fitting line shows that, penalties grow linearly with increase of modulation amplitude in both cases. We approximate the rRx penalty scaling factor as 3.145 dB/rad for phase modulation and 0.0315 dB per percent of amplitude modulation depth, which indicates the magnitude of changes in signal amplitude when amplitude modulation is applied. Both signal phase amplitude and amplitude modulation depth were multiplied by introduced scaling factors and summed up to simulate rOSNR penalty considering residual dithering on the receiver.

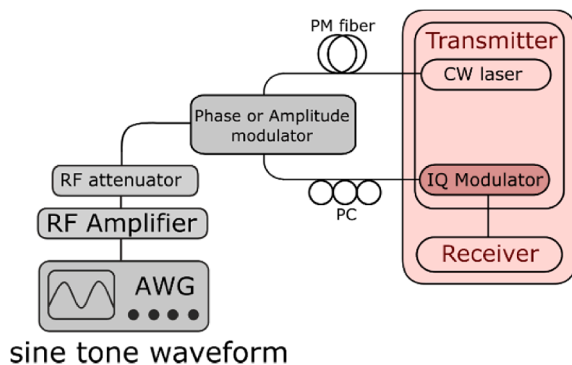


Fig. 8. Setup for characterization receiver penalty. AWG – arbitrary waveform generator, PC – polarization controller, PM fiber – polarization maintaining fiber.

#### 3.2. Experimental setup

Fig. 10 shows the experimental setup for evaluation of the PI-FOPA pump phase modulation impact on QAM signals.

A commercial transponder was used to generate a 35GBaud 200G PDM-16-QAM signal in the wavelength range from 1530 nm to 1547 nm covering the 3 dB FOPA gain bandwidth. The signal was passed through a polarization scrambler to provide a random change of polarization in time to compare results with simulation. The polarization scrambling speed was 20 krad/s which we confirmed to allow for penalty-free operation of the employed transponder in B2B configuration. Then, the signals were amplified by a PI-FOPA with net gain in the range from  $12 \pm 0.5$  dB to  $15 \pm 0.5$  dB across the examined wavelength range (corresponded on/off gain of  $17 \pm 0.5$  and  $20 \pm 0.5$  dB), with polarization-dependent gain (PDG) of less than 0.2 dB across all measurements. For B2B measurements used as a reference, the PI-FOPA has been bypassed. The signal was then passed through a variable optical attenuator (VOA) to ensure that the detected signal power was  $-7$  dBm for all BER measurements including B2B. Then, the signal was combined with an amplified spontaneous emission (ASE) noise, which power was varied with another VOA to sweep the OSNR. Then, the signal OSNR was measured through a tap coupler with an optical spectral analyzer (OSA). Finally, the signal was passed through a band pass filter (BPF) and then detected by a coherent receiver which measured BER via counting errors for 1 s.

The PI-FOPA architecture was as explained in section 2.3. The PI-FOPA pump was sourced from a 100 kHz linewidth laser at the wavelength 1566.2 nm. The pump was then phase modulated with a range of multi tone waveforms to examine their SBS mitigation capability and impact on an amplified signal. The multi-tone waveforms were generated by AWG and amplified with an RF amplifier. Each generated waveform consisted of three or four tones, whereas the base tone had frequency between 25 MHz and 225 MHz, and the rest of tones were obtained by subsequent multiplication by 3.05. The amplitudes of the tones produced by the AWG were adjusted so that all the first-order harmonics have equal power within a 1 dB variation, and this corresponds to the phase modulation amplitude of 1.4 rad per tone. The resulting pump bandwidth was between 2 GHz and 7 GHz. The tone frequency spacing and power distribution between them was observed at the 26.5 GHz RF spectrum analyzer by using a heterodyne method with a local oscillator which frequency was shifted by 8.9 GHz from the pump.

In the PI-FOPA, the phase-modulated pump was split into two arms via 3 dB coupler and amplified by high-power Erbium-Doped Fiber Amplifiers (EDFAs). We measured the delay between pumps by amplifying a 10 Gbit/s OOK signal with a  $(2^7 - 1)$  PRBS pattern in for each arm in turn, measuring the rising edge of the longest string of consecutive one symbols on Tektronix Oscilloscope. The delay between pumps was determined by comparing PRBS patterns saved from the two arms. The measured delay between PRBS patterns was  $20.56 \pm 0.02$  ns, corresponding to an optical path difference between the pumps of 4.1 m. The pump powers launched into the Highly Nonlinear Fibers (HNLFs) were approximately 38 dBm, and the HNLFs were 50 m long.

The SBS threshold increase for each examined phase modulation waveform was found by varying input pump power and measuring the backscattered pump power from power meters PM1 and PM2 respectively. Then, the backscattered-to-input pump power ratio was derived and, the SBS threshold was defined as the input pump power when this ratio was 35.5 dB, i.e., just above the level of linear backscattering/backreflection.

#### 3.3. Comparison of pump dithering waveforms

First, we experimentally found the SBS threshold increase facilitated by a range of examined phase modulation waveforms. The SBS threshold increase is defined as a difference between the SBS thresholds measured

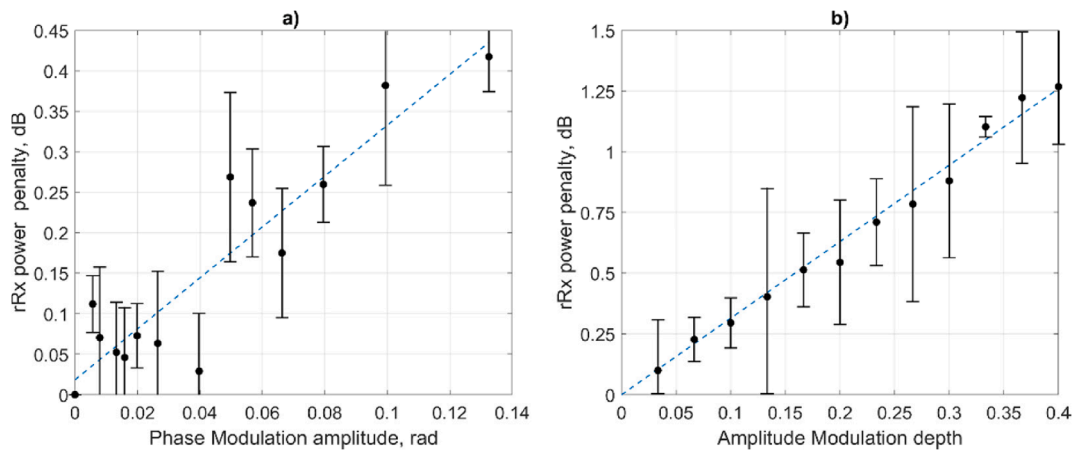


Fig. 9. A) required Rx power penalty vs phase modulation amplitude, b) required Rx power penalty vs amplitude modulation depth. Blue dashed line is linear fit. (For interpretation of the references to colour in this figure legend, the reader is referred to the web version of this article.)

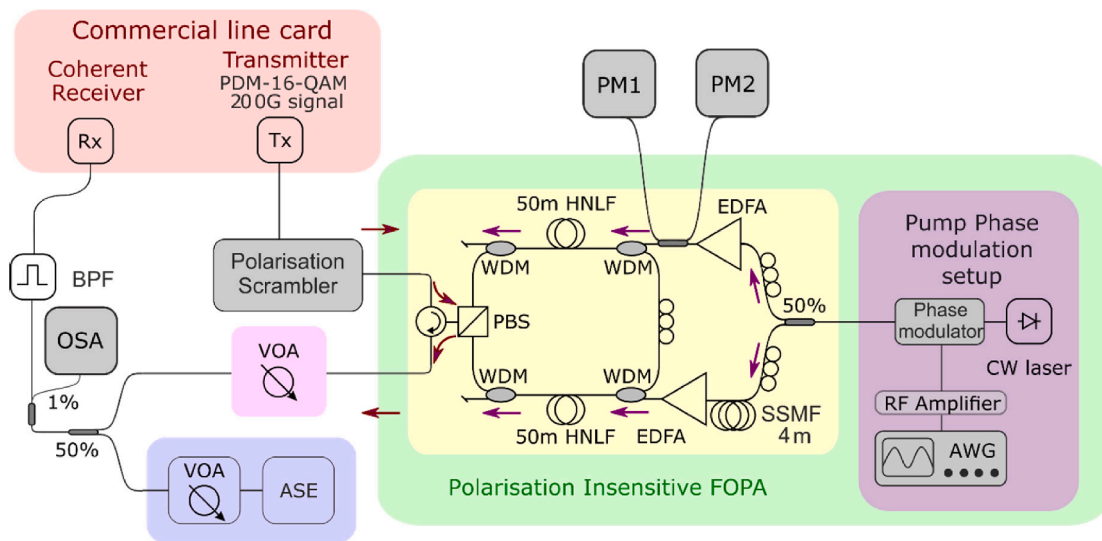


Fig. 10. Experimental setup: OSA – Optical spectrum analyzer, ESA – electrical spectrum analyzer, ASE – amplified spontaneous emission, BPF – bandpass filter, HNLF – highly nonlinear fiber, PM – power meter, AWG – arbitrary waveform generator, VOA – variable optical attenuator, PC – polarization controller.

for each scenario and the no dithering case when the SBS threshold was 25.5 dBm. Fig. 11(a) shows the SBS threshold increase measured for the range of generated in AWG pump waveforms modulated with three

(‘blue’) and four (‘red’) sine tones with the total bandwidth between 2 and 6.8 GHz. The total bandwidth was expanded by increasing the spacing between tones, achieved by raising the frequencies of the base

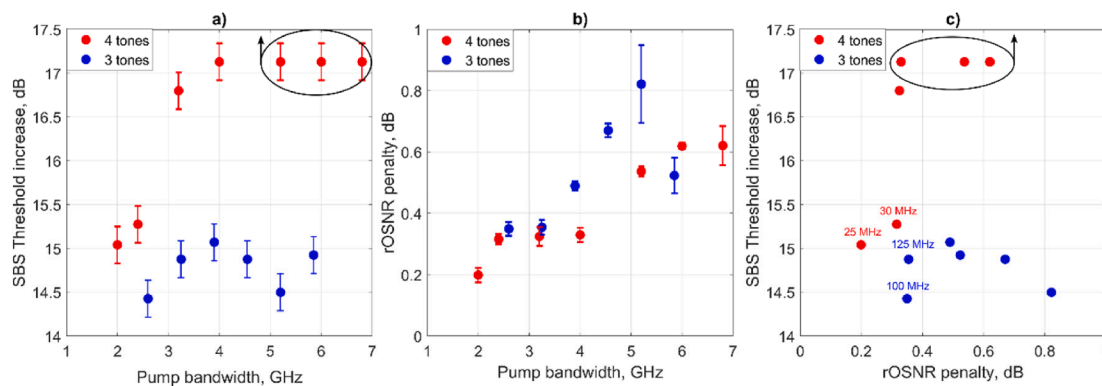


Fig. 11. A) sbs threshold increase vs pump bandwidth (note, it was not possible to measure values above 17 dB due to lack of pump power), b) rOSNR penalty vs pump bandwidth, c) SBS threshold increase vs rOSNR penalty. Signal wavelength 1545 nm. Blue dots – 3 sine tones with  $f_{\text{basetone}}$  in range between 100 MHz and 225 MHz. Red Dots – 4 sine tones with  $f_{\text{basetone}}$  in range between 25 MHz and 85 MHz. (For interpretation of the references to colour in this figure legend, the reader is referred to the web version of this article.)

tones. We have observed that in the three-tones case the increase in the SBS threshold was about 14.5 dB for all pump bandwidths. This corresponds to the factor of  $\sim 27$  as the pump was split into 27 lines separated by more than the SBS interaction bandwidth (minimal examined base frequency in this case was 100 MHz). In the four-tones case the SBS threshold increased linearly until pump bandwidth reached 4 GHz (base frequency of 50 MHz), and then the maximum EDFA power (43dBm) was not sufficient to induce an observable SBS, so the SBS threshold increase appears flat on the plot, but we expect it to reach  $\sim 19$  dB (factor of 81). In addition, these measurements experimentally confirmed that waveforms with more tones provide higher SBS suppression even for the same pump bandwidth because more tones allow for more uniform spectral power distribution.

The required-OSNR penalty was experimentally measured and determined at the BER level of 0.01 for each examined pump phase modulation waveform compared to back-to-back case for signal wavelength of 1545 nm. The OSNR penalty increases with the total pump bandwidth (see Fig. 11(b)) along the same trend for both three and four tones, so we conclude the OSNR penalty is defined by the pump bandwidth rather than by the number of tones or base frequencies.

Fig. 11(c) summarizes findings of Fig. 11(a) and (b) by plotting SBS threshold increase vs required-OSNR for each scenario: the waveform with 4 tones and base tone frequency of 25 MHz shows the rOSNR penalty of 0.19 dB and the SBS threshold increase by 15 dB as compared to the waveform commonly used by state-of-art FOPAs with 3 tones and base frequency of 100 MHz having the rOSNR penalty of 0.35 dB and the SBS threshold increase of 14.4 dB. This observation makes a strong case towards using a higher number of tones as it allows for better SBS suppression for the same rOSNR penalty or, correspondingly, less rOSNR penalty for the same SBS suppression.

### 3.4. The required signal OSNR penalty as a function of total pump bandwidth

In this subsection, we investigate the impact of pump dithering on

the required-OSNR penalty experimentally measured across several signal wavelengths as a function of total pump bandwidth and compare the results with our simulation to confirm our simulation model of PI-FOPA. In simulation, parameters were taken from Fig. 1 and description of experimental setup from subsection 3.2 to fit the experimental gain spectrum.

Fig. 12 demonstrates rOSNR penalty versus total pump bandwidth for 4 wavelengths across the 3 dB FOPA gain bandwidth. Experimental results shown with red dots and blue dots, follow the same trend of the rOSNR penalty increase with pump bandwidth demonstrated in 2.2, although experimental points show some scattering especially at 1531 nm (see Fig. 12 (a)). There are several potential reasons for this, including: we modeled the phase noise added by commercial receiver based on measurements taken with one sine tone, while pump was phase modulated with 3 or 4 tones. The second reason can be that modulation with four tones with smaller spacing between tones has impact similar to modulation with white noise, so the commercial receiver DSP easy to compensate for it. The linear slope increases with the signal wavelength detuning from the pump in accordance with the Fig. 2. The rOSNR penalty are about 0.2–0.4 dB at the 2 GHz pump bandwidth and increase up to 0.5—1 dB at 6.8 GHz. Therefore, the pump bandwidth has to be kept as low as possible for the best performance and then rOSNR penalties of signals amplified by a PI-FOPA can be kept low in the range of 0.2–0.4 dB even without dithering cancellation.

### 3.5. Mitigation of the dithering impact in PI-FOPA

Finally, to check if there is a potential of PI-FOPA architecture to mitigate impact of dithering discussed in 2.4, we adjusted pump phase modulation frequencies via AWG to take into account the de-facto delay between arms of 20.56 ns. We confirm this approach by varying the base tone frequency with step of 250 kHz and measured corresponding rOSNR penalty.

Fig. 13 shows rOSNR penalty versus pump base tone frequency for two examined signal wavelengths of 1531 nm and 1545 nm

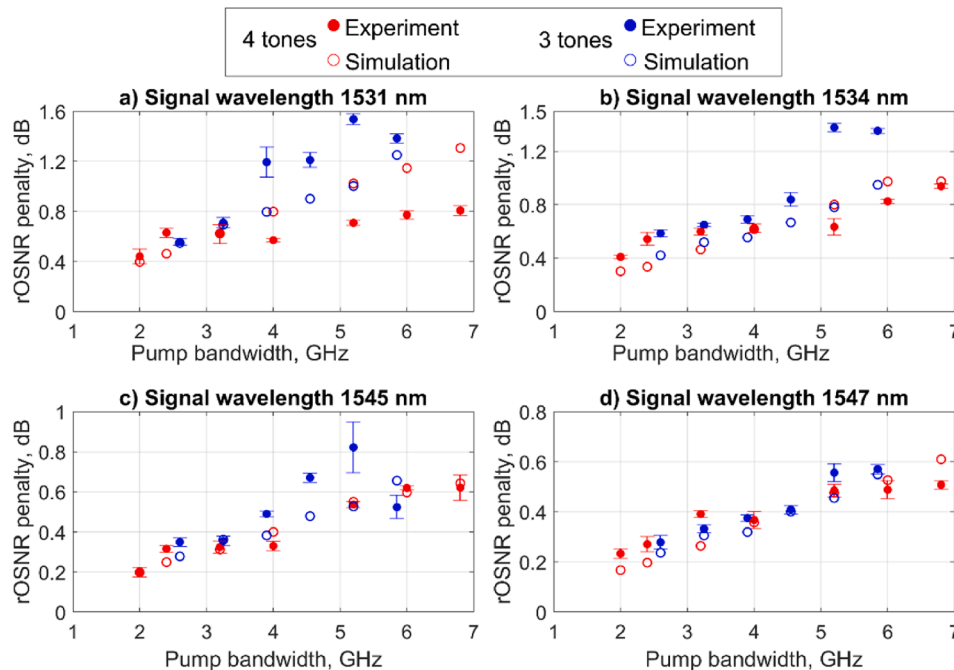


Fig. 12. Rosnr penalty versus total pump bandwidth for 4 wavelengths across 3 dB FOPA gain bandwidth. Red dots – experiment data with 4 sine tones with  $f_{\text{basitone}}$  in range between 25 MHz and 85 MHz, blue dots – experiment data with 3 sine tones with  $f_{\text{basitone}}$  in range between 100 MHz and 225 MHz, red circles – simulation with 4 sine tones with  $f_{\text{basitone}}$  in range between 25 MHz and 85 MHz, blue circles - simulation with 3 sine tones with  $f_{\text{basitone}}$  in range between 100 MHz and 225 MHz. FOPA parameters from Fig. 1,  $K = \text{random}$ , and including performance of real receivers. (For interpretation of the references to colour in this figure legend, the reader is referred to the web version of this article.)

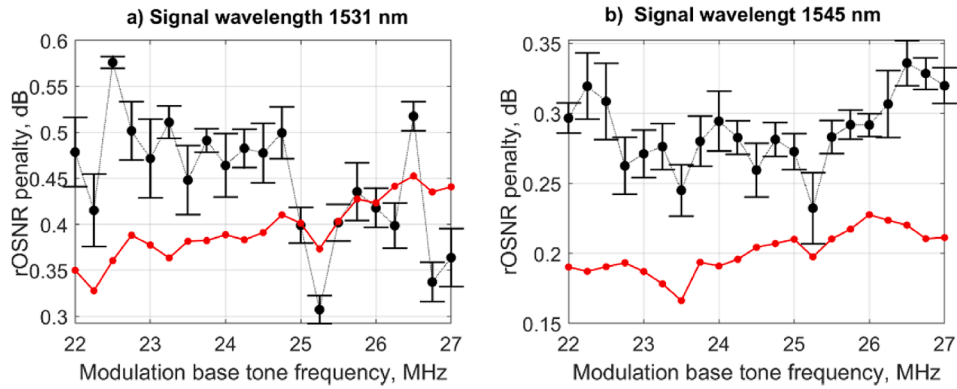


Fig. 13. rOSNR penalty vs Pump base tone frequency for signal wavelength of a) 1531 nm and b) 1545 nm. Black – experimental data with error bars, Red –simulation using the FOPA parameters from Fig. 1, K = random, and including performance of real receivers. (For interpretation of the references to colour in this figure legend, the reader is referred to the web version of this article.)

corresponding to the edges of the 3 dB FOPA gain bandwidth. Each experimental data point (depicted in black with error bars) represents an average obtained from an ensemble that includes all potential signal polarization states measured over a period of time. This period was the same for each base tone frequency within the range of 22 MHz to 27 MHz.

The two lowest experimentally measured penalties were observed at base tone frequencies of 23.5 MHz and 25.25 MHz as predicted by our simulation. Although experimental results might look like a random scatter, they are averaged across a number of measurements taken at different time, and the minimum penalty for both signal wavelengths occur exactly at the frequency where we expect the best cancelation for the measured delay between the pump paths. Therefore, we believe this is confirmation that performance improvement can be achieved by matching the pump phase modulation frequency with the time delay between pumps. The discrepancy between simulations and experiment, such as increased penalties being generally higher than theoretically ones, can be explained by impact of other penalty sources, such as nonlinear distortion.

3.6. rOSNR penalty distribution across the FOPA gain spectrum

Fig. 14 illustrates the rOSNR penalty as a function of signal

wavelength for 4 scenarios. The pumps were phase modulated with a combination of 4 sine tones, whereas the base tone was 25.25 MHz and higher frequencies were obtained via multiplication by 3.05, 3.05<sup>2</sup> and 3.05<sup>3</sup>. Blue curve represents an ideal receiver which penalties could be below 0.1 dB between 1530 nm and 1545 nm. However, experimental results (black) show much larger penalty, so we include the receiver penalty into our simulations. The penalty due to the amplitude modulation (green) exhibits a minimum at the FOPA gain peak of ~ 1534 nm, where gain spectrum is flat and so the induced amplitude gain fluctuation is the lowest as was shown in [32]. Similarly, the rOSNR penalty is the highest at the gain spectrum slope (see Fig. 2)), i.e., 1530 nm. Amplitude modulation is more pronounced at the spectrum edges of 1530 nm and 1548 nm leading to an increase in rOSNR penalty. The yellow curve shows how the commercial receiver adds penalty due to transferred phase modulation to the signals, which grows monotonically with the distance from the pump wavelength. Penalties at wavelengths closer to pump wavelength are mostly caused by residual signal amplitude modulation, while the distant wavelengths are exposed to the inherited signal phase modulation. The red curve summarizes the effect of both modulations and matches the experimental results shown by black dots very well although with a small additional penalty not reflected in the simulation. Deviation of experimental points from theoretical predictions near the peak (1532–1534 nm) is anomalous and

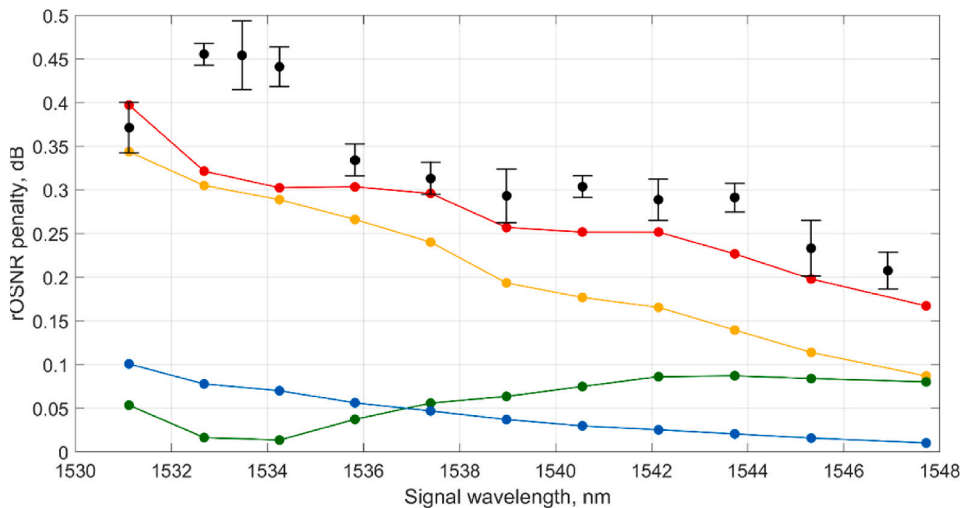


Fig. 14. rOSNR penalty vs signal wavelength. Red - simulated real receiver, Yellow – simulated real receiver considering only phase modulation, Green - simulated real receiver with only induced amplitude modulation, Blue –simulation of ideal receiver, Black – experiments. Simulation using the FOPA parameters from Fig. 1, K = random and including performance of real receivers. (For interpretation of the references to colour in this figure legend, the reader is referred to the web version of this article.)

cannot be explained by our model.

The measurement error of  $\sim 0.05$  dB in the required-OSNR penalty fluctuation is caused by several reasons, such as the OSNR measurement error, FOPA gain drifts, and polarization variations.

#### 4. Conclusion

This work has demonstrated the relationship between pump phase modulation employed for the SBS mitigation in polarization-diverse FOPAs and the resulting QAM signal degradation. While coherent detection of QAM signals decreases the impact of the signal amplitude modulation induced by the pump phase modulation, QAM signals are susceptible to the induced signal phase modulation. The total pump bandwidth should be minimized to reduce the required-OSNR penalty, and this can be done without compromising the SBS mitigation by employment of larger number of tones with less spacing between the tones. We have shown that waveforms based on 4 tones with total pump bandwidth of 2086 MHz can allow for 0.5 dB higher SBS threshold increase and  $\sim 0.15$  dB less required-OSNR penalty than waveforms based on 3 tones with total pump bandwidth of 2670 MHz.

Through simulations and experiments, we explored the required-OSNR penalty distribution across the FOPA gain spectrum and found that it differs significantly from what was previously reported for the on/off keying signals. We have observed that receiver DSP plays significant role in contributing to penalties as an ideal simulated receiver could allow for much lower signal penalties.

Polarization diverse architecture makes the impact of pump phase modulation more complicated as signals propagate along two different spatial paths and inherit modulation of two different pumps before being recombined. This, however, allows for reduction of the required-OSNR penalty by up to 0.1–0.2 dB if the pump phase modulation frequencies and/or mismatch between the pump's optical paths are adjusted.

#### CRedit authorship contribution statement

**M. Bastamova:** Writing – original draft, Visualization, Methodology, Investigation, Formal analysis, Conceptualization. **V. Gordienko:** Writing – review & editing, Writing – original draft, Methodology, Investigation, Formal analysis, Conceptualization. **N.J. Doran:** Supervision, Project administration, Conceptualization. **A.D. Ellis:** Writing – review & editing, Supervision, Methodology, Funding acquisition, Conceptualization.

#### Declaration of competing interest

The authors declare the following financial interests/personal relationships which may be considered as potential competing interests: Vladimir Gordienko reports equipment, drugs, or supplies was provided by Ciena Corporation. Vladimir Gordienko reports equipment, drugs, or supplies was provided by Furukawa Electric Group. If there are other authors, they declare that they have no known competing financial interests or personal relationships that could have appeared to influence the work reported in this paper.

#### Data availability

Data underlying the results presented in this paper are available in <https://doi.org/10.17036/researchdata.aston.ac.uk.00000618>

#### Acknowledgements

We wish to thank Dr Shigehiro Takasaka and Dr Ryuichi Sugizaki of Furukawa Electric for highly nonlinear fibers, and Dr Charles Laperle of Ciena for the transponder. This work was funded by the EPSRC projects EP/S016171/1 (EEMC) and EP/T518128/1 (DTP). Data underlying the

results presented in this paper are available in Ref. [41].

#### References

- [1] N. Deng, L. Zong, H. Jiang, Y. Duan, K. Zhang, Challenges and enabling Technologies for Multi-Band WDM optical networks, *J. Light. Technol.* 40 (11) (2022) 3385–3394, <https://doi.org/10.1109/JLT.2022.3162725>.
- [2] Z. Zhai, A. Halder, J. Sahu, “E+S-band Bismuth-doped Fiber Amplifier with 40dB Gain and 1.14dB Gain per Unit Length,” *Eur. Conf. Opt. Commun. (ECOC 2023)*, pp. 1–3, 2023.
- [3] A. Donodin, V. Dvoyrin, E. Manuylovich, L. Krzczanowicz, W. Forsysiak, M. Melkumov, V. Mashinsky, S. Turitsyn, Bismuth doped fibre amplifier operating in E-and S-optical bands, *Optical Materials Express* 11 (1) (2021) 127–135.
- [4] P. Hazarika, M. Tan, A. Donodin, S. Noor, I. Phillips, P. Harper, J.S. Stone, M.J. Li, W. Forsysiak, E-, S-, C-and L-band coherent transmission with a multistage discrete raman amplifier, *Optics Express* 30 (24) (2022) 43118–43126.
- [5] M.E. Marhic, K.-K.-Y. Wong, L.G. Kazovsky, Wide-band tuning of the gain spectra of one-pump fiber optical parametric amplifiers, *IEEE Journal of Selected Topics in Quantum Electronics* 10 (5) (2004) 1133–1141.
- [6] V. Gordienko, M.F.C. Stephens, A.E. El-Taher, N.J. Doran, Ultra-flat wideband single-pump raman-enhanced parametric amplification, *Opt. Express* 25 (5) (2017) 4810–4818.
- [7] M.E. Marhic, *Fiber optical parametric amplifiers*, in: *Oscillators and Related Devices*, Cambridge University Press, 2008, <https://doi.org/10.1017/CBO9780511600265>.
- [8] M.E. Marhic, P.A. Andrekson, P. Petropoulos, S. Radic, C. Peucheret, M. Jazayerifar, Fiber optical parametric amplifiers in optical communication systems, *Laser Photonics Rev.* 9 (1) (2015) 50–74, <https://doi.org/10.1002/lpor.201400087>.
- [9] M.F.C. Stephens, V. Gordienko, N.J. Doran, 20 dB net-gain polarization-insensitive fiber optical parametric amplifier with >2 THz bandwidth, *Opt. Express* 25 (9) (2017) 10597–10609.
- [10] C. B. Gaur, V. Gordienko, P. Hazarika, and N. J. Doran “Polarization Insensitive Fiber Optic Parametric Amplifier with a Gain Bandwidth of 22 nm in S-Band,” *Opt. Fiber Commun. Conf. (OFC 2022)*, W4J-1. Optica Publishing Group, 2022. 10.1364/OFC.2022.W4J.1.
- [11] V. Gordienko, C. B. Gaur, F. Bessin, I. D. Phillips and N. J. Doran, “Robust polarization-insensitive C & L band FOPA with >17dB gain for both WDM and bursty traffic,” in *Optical Fiber Communications Conference and Exhibition (OFC)*, San Francisco, CA, USA, 2021, paper M5B.3.
- [12] T. Zhi, C. Lundström, P.A. Andrekson, C.J. McKinstry, M. Karlsson, D.J. Blessing, E. Tipsuwanakul, B.J. Puttnam, H. Toda, L. Grüner-Nielsen, Towards ultrasensitive optical links enabled by low-noise phase-sensitive amplifiers, *Nat. Photonics* 5 (7) (2011) 430–436, <https://doi.org/10.1038/nphoton.2011.79>.
- [13] V. Gordienko, F. Ferreira, J. R. Lamb, A. Szabo, and N. Doran, “Phase-sensitive amplification of 11 WDM channels across bandwidth of 8 nm in a fibre optic parametric amplifier,” *2020 Eur. Conf. Opt. Commun. (ECOC 2020)*, no. 1, pp. 2–5, 2020, 10.1109/ECOC48923.2020.9333194.
- [14] T. Torounidis, P.A. Andrekson, B.E. Olsson, Fiber-optical parametric amplifier with 70-dB gain, *IEEE Photonics Technol. Lett.* 18 (10) (2006) 1194–1196, <https://doi.org/10.1109/LPT.2006.874714>.
- [15] C.B. Gaur, V. Gordienko, F. Ferreira, V. Ribeiro, N.J. Doran, Fibre optic parametric amplifier for high capacity burst-mode access networks, *Opt. Express* 29 (14) (2021) 21190–21198, <https://doi.org/10.1364/oe.422990>.
- [16] C.B. Gaur, F. Ferreira, V. Gordienko, A. Iqbal, W. Forsysiak, N. Doran, Experimental comparison of fiber optic parametric, raman and erbium amplifiers for burst traffic for extended reach PONs, *Opt. Express* 28 (13) (2020) 19362–19373, <https://doi.org/10.1364/OE.394379>.
- [17] V. Gordienko, F.M. Ferreira, C.B. Gaur, N.J. Doran, Looped Polarization-insensitive fiber optical Parametric amplifiers for broadband high gain applications, *J. Light. Technol.* 39 (19) (2021) 6045–6053, <https://doi.org/10.1109/JLT.2021.3099441>.
- [18] E.P. Ippen, R.H. Stolen, Stimulated Brillouin scattering in optical fibers, *Appl. Phys. Lett.* 21 (11) (1972) 539–541, <https://doi.org/10.1063/1.1654249>.
- [19] V. Gordienko, D. Szabó, M.F.C. Stephens, V. Vassiliev, C.B. Gaur, N.J. Doran, Limits of broadband fiber optic parametric devices due to stimulated Brillouin scattering, *Opt. Fiber Technol.* 66 (January) (2021) 2–6, <https://doi.org/10.1016/j.yofte.2021.102646>.
- [20] K. Shiraki, M. Ohashi, M. Tateda, Suppression of stimulated Brillouin scattering in a fibre by changing the core radius, *Electronics Letters* 31 (8) (1995) 668–669, <https://doi.org/10.1049/el:19950418>.
- [21] L. Ming-Jun, X. Chen, J. Wang, S. Gray, A. Liu, J.A. Demeritt, A. Boh Ruffin, A. M. Crowley, D.T. Walton, L.A. Zenteno, Al/Ge co-doped large mode area fiber with high SBS threshold, *Opt. Express* 15 (13) (2007) 8290–8299, <https://doi.org/10.1364/oe.15.008290>.
- [22] J. Hansryd, F. Dross, M. Westlund, P.A. Andrekson, S.N. Knudsen, Increase of the SBS threshold in a short highly nonlinear fiber by applying a temperature distribution, *J. Light. Technol.* 19 (11) (2001) 1691–1697, <https://doi.org/10.1109/50.964069>.
- [23] C. Guo, M. Vasilyev, Y. Akasaka, P. Palacharla, S. Takasaka, and R. Sugizaki, “Temperature-tuned two-segment highly-nonlinear fiber with increased stimulated Brillouin scattering threshold,” *Optical Fiber Communications Conference and Exhibition (OFC 2023)*, pp. 1–3, 2023, 10.23919/OFC49934.2023.10116506.
- [24] P. D. Dragic, C. H. Liu, G. C. Papen, and A. Galvanuskas, “Optical fiber with an acoustic guiding layer for stimulated Brillouin scattering suppression,” (CLEO).

- Conference on Lasers and Electro-Optics, vol. 3, pp. 1984-1986. IEEE, 2005, 10.1109/cleo.2005.202342.
- [25] J.M. Chavez Boggio, J.D. Marconi, H.L. Fragnito, Experimental and numerical investigation of the SBS-threshold increase in an optical fiber by applying strain distributions, *J. Light. Technol.* 23 (11) (2005) 3808–3814, <https://doi.org/10.1109/JLT.2005.856226>.
- [26] K.Y.K. Wong, K. Shimizu, K. Uesaka, G. Kalogerakis, M.E. Marhic, L.G. Kazovsky, Continuous-wave fiber optical parametric amplifier with 60 dB gain using a novel two-segment design, *OSA Trends Opt. Photonics Ser.* 88 (12) (2003) 1115–1116.
- [27] H. Lee, G.P. Agrawal, Suppression of stimulated brillouin scattering in optical fibers using fiber bragg gratings, *Opt. Express* 11 (25) (2003) 3467–3472, <https://doi.org/10.1364/ol.401433>.
- [28] J. Coles, *Advanced phase modulation techniques for stimulated brillouin scattering suppression in fiber optic parametric amplifiers*, University of California, San Diego, 2009.
- [29] J.B. Coles, et al., Bandwidth-efficient phase modulation techniques for stimulated brillouin scattering suppression in fiber optic parametric amplifiers, *Opt. Express* 18 (17) (2010) 18138–18150, <https://doi.org/10.1364/oe.18.018138>.
- [30] M.C. Ho, M.E. Marhic, K.Y.K. Wong, L.G. Kazovsky, Narrow-linewidth idler generation in fiber four-wave mixing and parametric amplification by dithering two pumps in opposition of phase, *J. Light. Technol.* 20 (3) (2002) 469–476, <https://doi.org/10.1109/50.988996>.
- [31] S. Radic, C.J. McKinstrie, R.M. Jopson, A.H. Gnauck, J.C. Centanni, A. R. Chraplyvy, Performance of fiber Parametric-processing Devices using Binary-phase-shift-keyed pump modulation, *IEEE Photonics Technol. Lett.* 16 (2) (2004) 548–550, <https://doi.org/10.1109/LPT.2003.823096>.
- [32] J.M.C. Boggio, A. Guimarães, F.A. Callegari, J.D. Marconi, H.L. Fragnito, Q penalties due to pump phase modulation and pump RIN in fiber optic parametric amplifiers with non-uniform dispersion, *Opt. Commun.* 249 (4–6) (2005) 451–472, <https://doi.org/10.1016/j.optcom.2005.01.056>.
- [33] A. Mussot, M. Le Parquier, P. Szriftgiser, Thermal noise for SBS suppression in fiber optical parametric amplifiers, *Opt. Commun.* 283 (12) (2010) 2607–2610, <https://doi.org/10.1016/j.optcom.2010.02.007>.
- [34] A. Vedadi, A. Mussot, E. Lantz, H. Maillotte, T. Sylvestre, Theoretical study of gain distortions in dual-pump fiber optical parametric amplifiers, *Opt. Commun.* 267 (1) (2006) 244–252, <https://doi.org/10.1016/j.optcom.2006.05.074>.
- [35] M. F. C. Stephens, A. Redyuk, S. Sygletos, I. D. Phillips, P. Harper, K. J. Blow, and N. J. Doran., “The impact of pump phase-modulation and filtering on WDM signals in a fibre optical parametric amplifier,” *Opt. Fiber Commun. Conf. (OFC 2015)*, vol. 2, no. 1, pp. 15–17, 2015, 10.1364/ofc.2015.w2a.43.
- [36] A. Mussot, A. Durécu-Legrand, E. Lantz, C. Simonneau, D. Bayart, H. Maillotte, and T. Sylvestre., “Influence of the phase modulation of the pump wave in fiber optical parametric amplifiers,” *Nonlinear Guided Waves and Their Applications*, p. MC20. Optica Publishing Group, 2004, 10.1364/nlgw.2004.mc20.
- [37] M. Bastamova, V. Gordienko, and A. Ellis, “Impact of Pump Phase Modulation on Fibre Optical Parametric Amplifier Performance for 16-QAM Signal Amplification,” *Eur. Conf. Opt. Commun. (ECOC 2022)*, paper Tu5.6. 2022, doi:org/10.17036/researchdata.aston.ac.uk.00000547.
- [38] M. Deroh, J.-C. Beugnot, K. Hammani, C. Finot, F. Julien Fatome, H.M. Smechtala, T. Sylvestre, B. Kibler, Comparative analysis of stimulated brillouin scattering at 2  $\mu\text{m}$  in various infrared glass-based optical fibers, *J. Opt. Soc. Am. B* 37 (12) (2020) 3792–3800, <https://doi.org/10.1364/josab.401252>.
- [39] D.G.M. Barry, R. John, E.A. Lee, *Digital communication*, Springer Science & Business Media, 2012.
- [40] B. Koch, R. Noé, D. Sandel, V. Mirvoda, Versatile endless optical polarization controller/tracker/demultiplexer, *Opt. Express* 22 (7) (2014) 8259–8276, <https://doi.org/10.1364/oe.22.008259>.
- [41] M. Bastamova, V. Gordienko, N.J. Dorand, A.D. Ellis, *Impact of pump phase modulation on QAM signals in Polarization-insensitive fiber optical Parametric amplifiers*, Aston University, 2023.